C. R. Chimie 19 (2016) 1580–1585

Contents lists available at ScienceDirect

Comptes Rendus Chimie

www.sciencedirect.com

Full paper/Mémoire

How to assess the role of Pt and Zn in the nephrotoxicity of Pt anti-cancer drugs? An investigation combining μXRF and statistical analysis: Part I: On mice

Emmanuel Estève [a], Dominique Bazin [c, d, *], Chantal Jouanneau [a], Stephan Rouzière [d], Aurélien Bataille [a], Alex Kellum [c], Karine Provost [e], Christian Mocuta [f], Solenn Reguer [f], Dominique Thiaudière [f], Kris Jorissen [g], John J. Rehr [g], Alexandre Hertig [a, h], Éric Rondeau [a, h], Emmanuel Letavernier [a, b], Michel Daudon [a, b], Pierre Ronco [a, b]

[a] UMR S1155, INSERM/UPMC, 4, rue de la Chine, 75970 Paris cedex 20, France
[b] AP-HP, Hôpital Tenon, Service d'Explorations Fonctionnelles, 4, rue de la Chine, 75970 Paris cedex 20, France
[c] CNRS, LCMCP-UPMC, Collège de France, 11, place Marcelin-Berthelot, 75231 Paris cedex 05, France
[d] Laboratoire de Physique des Solides, UMR 8502, CNRS, Bât. 510, Université Paris-11, 91405 Orsay, France
[e] Institut de Chimie des Matériaux Paris Est, UMR 7182, CNRS, UPEC, 2–8, rue Henri-Dunant, 94320 Thiais, France
[f] Synchrotron SOLEIL, L'Orme des Merisiers, Saint-Aubin, BP 48, 91192 Gif-sur-Yvette, France
[g] Department of Physics, University of Washington, Seattle, Washington, 98195, USA
[h] AP-HP, Hôpital Tenon, Service UNTR, 4, rue de la Chine, 75970 Paris cedex 20, France

ARTICLE INFO

Article history:
Received 21 October 2015
Accepted 17 March 2016
Available online 22 April 2016

Keywords:
Cancer
Pt anticancer drugs
Nephrotoxicity

ABSTRACT

Nephrotoxicity is a specific and serious adverse effect of cisplatin which limits its utilization. Here we present an experimental approach to decipher its mechanisms focusing on the renal distribution of Pt and Zn in cisplatin exposed mice kidneys. We combined Synchrotron Radiation (S.R.) μX-ray fluorescence with statistical treatments. μX-ray fluorescence data were collected on a set of mice biopsies after cisplatin, oxaliplatin and carboplatin injections. Even if this investigation is based on a limited number of samples, these preliminary data seem to reveal a stronger correlation between the spatial repartition of Pt and Zn for cisplatin than for the other Pt containing drugs. The cisplatin injection induced a redistribution of medullary Zn across the corticomedullary junction where histological lesions develop. These results were confirmed by evaluation of Pearson's and Manders' co-localization coefficients. These data suggest that Zn is involved in the nephrotoxicity of cisplatin. This could lead to new diagnosis, physiopathological and even therapeutical approaches.

1. Introduction

Each year in Europe, 3.45 million new cases of cancer (excluding non-melanoma skin cancer) are diagnosed, and 1.75 million patients die. Breast (464,000 cases), colorectal (447,000), prostate (417,000) and lung (410,000) cancers are the most common [1]. Platinum-based anticancer drugs, first introduced in clinical practice as cisplatin, a square-planar platinum (II) complex [2], are now largely used as anti-cancer agents in many solid organ malignancies including those of testis, thyroid, breast, colon and

* Corresponding author.
E-mail address: Dominique.bazin@upmc.fr (D. Bazin).

http://dx.doi.org/10.1016/j.crci.2016.03.014

rectum. Although thousands of platinum complexes have been synthesized and evaluated for their anticancer activity [3], only a few have entered clinical trials. Among them, cisplatin and carboplatin are used world-wide, oxaliplatin in a few countries, nedaplatin in Japan, heptaplatin in the Republic of Korea, and Lobaplatin in China [3–6]. All these Pt molecules display the same putative pharmacological mode of action. Pt(II) complexes are supposed to form adducts with amine groups of proteins, RNA and DNA. The bending of the DNA strand impedes proper DNA transcription leading to cell death [7–9]. The mode of action of Pt(II) molecules is still the object of active research [9,10]. The search for new Pt anti-cancer drugs [11,12] is driven by the need to overcome cytotoxicity [13–15], adverse effects and limited tumor penetration of existing platinum agents [16], as well as intrinsic and acquired resistance [17]. In addition to ototoxicity, gastrotoxicity, myelosuppression, and allergic reactions [18–20], the main dose-limiting adverse effect of cisplatin is nephrotoxicity [21–23]. A number of investigations have been performed on cells in a monolayer culture, but these experimental conditions are far from the tumor microenvironment where cells are exposed to heterogeneous conditions (large concentration gradient as the drug diffuses from the blood vessels) [11].

The hallmark feature of cisplatin-induced nephrotoxicity is an acute tubular necrosis affecting mainly proximal tubular cells, resulting in acute renal failure. Cisplatin-induced nephrotoxicity is mediated by binding with thiol-containing enzymes which can lead to oxidative stress and subsequent cell injury [3–6]. However, although Pt salts are chemically very close to each other, they show various degrees of efficacy and toxicity. For instance, nephrotoxicity is a major limitation to the current use of cisplatin but remains exceptional with oxaliplatin or carboplatin. Our goal is to investigate inflammation and nephrotoxicity induced by these drugs using new experimental approaches to provide clinicians with improved guidelines. Convergent data reviewed [24] indicate a relationship between Zn and inflammation, which led us to investigate the spatial relationship between Pt and Zn in Pt salt exposed kidney.

In the first step presented in this paper, we injected mice with cisplatin, oxaliplatin and carboplatin and studied the spatial distribution of Pt and Zn in their kidneys using synchrotron radiation (S.R.) as the probe. More precisely, S.R.- μX-ray Fluorescence (SR-μXRF) data [25–29] were processed and Pearson's and Manders' co-localization coefficients were calculated. This allowed us to obtain a micrometer scale resolution [30–34].

2. Material and methods

Briefly, 20-g C57/Black6 female mice (Charles River, USA) were injected intraperiteonally with 13 mg/kg equivalent Pt. Mice 1 and 2 were given 24.7 mg/kg carboplatin (Hospira France, France); mice 3 and 4, 20 mg/kg cisplatin (Mylan pharmaceutics, USA); mice 5 and 6, 26.5 mg/kg oxaliplatin (Accord Healthcare Ltd, UK). Kidneys were sampled on day 3 at the onset of acute kidney injury. Finally, the kidney tissues are processed into paraffin. All the experiments are performed on tissue sections.

All samples were investigated on the DiffAbs beamline at Synchrotron SOLEIL (France). This equipment is mainly dedicated to structural characterization by X-ray diffraction, X-ray absorption (XAS), and X-ray fluorescence (XRF) spectroscopy. The monochromator, the mirror as well as the devices used for the detection on DiffAbs, were reported in previous studies at the interface between medicine and physics [35–40].

A Kirkpatrick-Baez (KB) focusing device [41] was used in order to obtain a micron-sized X-ray beam. It consists of two orthogonally placed curved mirrors, illuminated at a glancing incident angle (about 0.2°). If the mirrors have an appropriate shape, the impinging X-ray beam (which can be considered almost parallel) is focused down to micrometer sizes. Two bending mechanisms are placed at each end of each mirror to monitor and change their curvature [42,43]. As a consequence, the resulting X-ray focused spot can be optimized in terms of intensity (photon flux) and size, depending on the experimental requirements (lateral resolution during sampling, concentration of chemical elements to be detected, etc.). The result was a clean, focused X-ray beam with an elliptic shape and a size of about 7 × 10 μm^2 (full width at half maximum, vertical × horizontal, FWHM) and a photon flux of several 10^9 ph in the spot.

We also point out the achromatic character of the KB focusing optics: the position and shape of the focal spot do not change when the X-ray energy is changed for absorption spectroscopy measurements. This makes the KB optics the best choice for local probe spectroscopy measurements (μXAS, μEXAFS or μXANES, but adapted as well for μXRF).

Analysis of the fluorescence spectra was performed using the tools of the PyMca software suite [44]. Energy calibration and a fitting procedure of the fluorescence lines for each spectrum allowed us to identify and evaluate the contribution of each element as shown in Fig. 2. Fluorescence maps of the four elements (Fe, Cu, Zn, Pt) correspond to the calculated area of the main fluorescence lines fitted with a Gaussian lineshape (Fe Kα, Cu Kα, Zn Kα, Pt Lα). In order to single out the Pt Lα, a Gaussian lineshape was used with a constant half-width at half-maximum of the peak (HWHM, this corresponds to a region of interest) of 50 eV allowing us to remove the Zn Kβ contribution. The same HWHM was used for the fitting procedure of the fluorescence lines of the three other elements.

This signal was used to generate maps representing Zn and Pt spatial distribution in our samples. The cortico-medullary junction was represented on these maps considering that the thickness of the normal female mouse cortex and medulla is 1.26 mm and 2.4 mm, respectively [45].

The fluorescence maps for the different samples and various chemical species were analyzed using Intensity Correlation Analysis methods [42,43] in order to highlight possible correlations related to the presence of the various chemical species in the tissue. Before describing the results, let us briefly describe the approach.

Consider two images (image 1 and image 2) of the same size (same number of points), obtained for two different species but the same sample, and let us denote by $X_{i,j}$ and

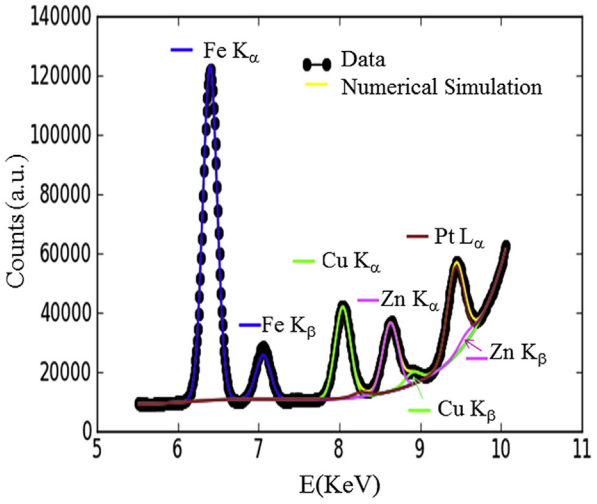

Fig. 1. XRF spectrum in the 5 − 10 keV range with the different contributions fitted. Special attention has been paid to distinguish the respective contributions of Zn ($K_\beta = 9572$ eV) and Pt ($L_\alpha = 9572$ eV) in the region of interest, namely between 9 and 10 KeV.

$Y_{i,j}$ the intensity of the pixel of coordinates (i,j) for the two images, respectively.

The Pearson co-localization coefficient is defined as:

$$r_p = \frac{\sum (X_{i,j} - X)(Y_{i,j} - Y)}{\sqrt{\sum (X_{i,j} - X)^2 \sum (Y_{i,j} - Y)^2}}$$

with the summations performed over the entire image, i.e., all the pixels of coordinates (i,j), and X and Y the average intensity for the two images, respectively. The obtained correlation of the intensity distribution in the two images is thus independent of the brightness. With this definition, r_p takes values from -1 to $+1$. A value of r_p close to 1 means that the images are strongly correlated or there is a good co-localization of the signal in the two images (brighter areas in image 1 correspond to brighter areas in image 2), while $r_p \approx 0$ is a signature of no correlation of the 2 images. We also note the case of r_p close to -1, in which case the images are negatively correlated (excluded), i.e., with reversed contrast (image 2 is the negative of image 1): brighter areas in image 1 correspond to darker areas in image 2 and vice versa. In the following, we will use the Pearson co-localization coefficient on the investigated object only, i.e., the images are first background corrected (background is calculated outside the measured object) and then the above summations are performed only inside the sample (for the pixels (i,j) for which $X_{i,j} > 0$ or $Y_{i,j} > 0$). The interpretation of the results based only on the Pearson coefficient might give rise to controversy: the results are sensitive to noise and are reliable only for high correlation (which is not necessarily the case for the samples depicted in this paper).

In order to push this analysis further, other coefficients and correlation maps can be calculated. We will focus here also on the Manders' coefficients (M1 and M2): we would like to know how well the intense pixels, above a certain intensity threshold, in image 1 co-localizes with intense pixels in image 2 (i.e. the probability to find bright pixels in image 2 only at the positions of intense pixels in image 1) and vice versa. It might be, for example, that a great part (or all) of the intense pixels of image 1 corresponds to intense pixels in image 2 (M1 ~ 1), but the opposite is not totally true: regions of the bright signal in the second image might not have any correspondence to image 1 (M2 << 1). Thus, the two approaches (Pearson and Manders) are not equivalent, and give complementary information.

3. Results and discussion

Platinum-based drugs are widely employed as anticancer agents because of their efficacy against a variety of tumors, but their use is limited by their nephrotoxicity. Here, we used a combination of sophisticated physics techniques to compare the spatial distribution and environment of Pt in mouse kidney tissue after intraperitoneal injection of three of these drugs selected for their varying renal toxicity. The results show that X-ray fluorescence can detect Pt in the cortex and the medulla of kidneys of Pt-salt exposed mice and that cisplatin is the only Pt salt that induces a redistribution of Zn in the cortex.

We first verified that using X-ray fluorescence experiments, we could identify trace elements including Iron, Copper, Zinc and Platinum (Fig. 1), and isolate by mathematical fitting the respective contributions of Pt Lα and Zn Kβ (which is extrapolated from Zn Kα), (Fig. 1). After injection to mice of the three Pt containing drugs, we showed that it was possible to visualize the respective spatial distribution of Zn and Pt (Fig. 2A–C).

In mice injected with carboplatin, Pt was detected evenly in the cortex, the medulla and at the corticomedullary junction (Fig. 2A and Supplementary Fig. 1). In contrast, Zn was almost restricted to the medulla, prevailing in the inner medulla. The pattern was different in mice injected with cisplatin. In these mice, Pt was also detected in the whole sample although it seemed to accumulate in the medulla (Fig. 2B). Interestingly, the Zn distribution pattern was changed and Zn was not only detected in the medulla but also in the cortex. In mice injected with oxaliplatin, Pt accumulated mostly around the corticomedullary junction whereas Zn was only found in the medulla (Fig. 2C).

Other investigators have assessed the role of Zn in the nephrotoxicity of Pt anti-cancer drugs. By using laser ablation inductively coupled plasma mass spectrometry (LA-ICP-MS), Moreno-Gordaliza et al. [46] showed that Pt accumulated in the kidney cortex, at the corticomedullary junction, and in the medullar pyramids. The deep cortex contains proximal tubule S3 segments, which are most sensitive to cisplatin nephrotoxicity. These authors also showed that the Zn distribution pattern was modified by Pt exposure but in their hands, Pt and Zn seemed to be anticorrelated. This might be due to different experimental protocols. Because we used mice whereas they used rats, we cannot exclude a different handling of Pt between the two species. They studied rats at two time points (3 days for 5 mg/kg and 5 days for 16 mg/kg) while we investigated mice 3 days after injection of 20 mg/kg. The observed

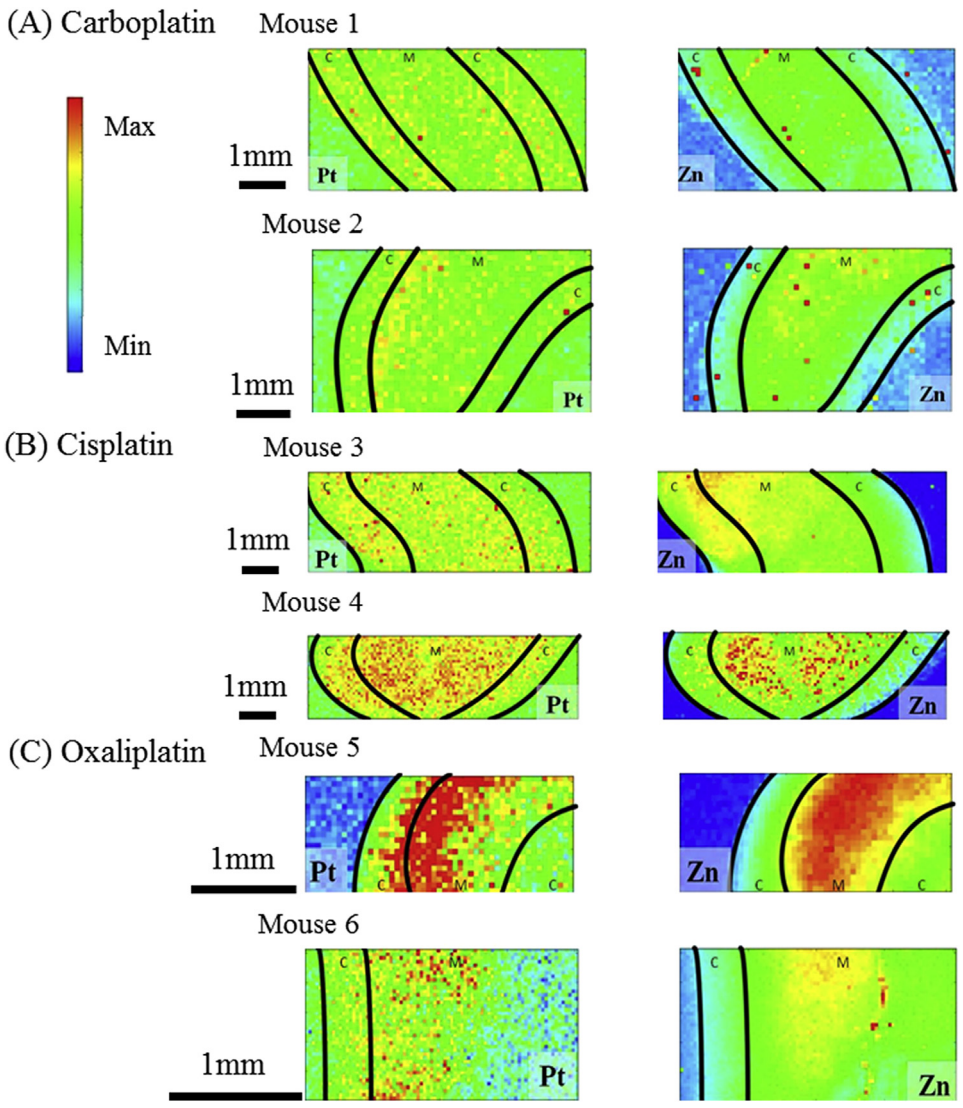

Fig. 2. (A) Carboplatin. 30 μm × 60 μm Zn and Pt XRF maps collected for the sample Mouse (B) Cisplatin 30 μm × 60 μm Zn and Pt XRF maps collected for the sample Mouse 3. (C) Oxaliplatin 30 μm × 60 μm Zn and Pt XRF maps collected for the sample Mouse 6. Black line denotes the sample limits and the cortico-medullary junction. C: Cortex, M: Medulla.

differences might also reflect the kinetics of Pt clearance and different steps of Pt induced inflammation.

One strength of our study is the combination of S.R.-μXRF at the micrometer scale with statistical treatments. We determined Pearson's and Mander's coefficients in order to evaluate possible spatial correlation between Pt and Zn species. The results show that such a spatial correlation exists but depends on the nature of Pt drugs which have been used, with the highest correlation being found for cisplatin (Fig. 3). This result is in full agreement with the detection of Zn in the cortex after cisplatin injection but not after oxali- or carboplatin injection.

The fact that only cisplatin-induced a redistribution of Zn to the cortex is of major interest, considering the role of Zn in inflammation [47–50]. Dietary zinc is an important immunoregulatory agent, a growth cofactor, and a cyto-protectant with anti-oxidant, anti-apoptotic, and anti-inflammatory roles [49]. Moreover, zinc picolinate might be a potential preventive agent in cisplatin-induced renal injury through decreasing oxidative stress and inflammation [50].

Whether the zinc we measured is linked to a modification in zinc renal metabolism, to the activation of protective mechanisms involved in heavy metal detoxification with metallothionein induction, or reflects the recruitment of platin induced damaged DNA linked proteins such as ZNF143, or accumulation of profibrotic metalloproteases such as MeprinA is unclear.

The present study has limitations. It was limited to a small number of mice which received a single dose at a single time point. We chose a dose of cisplatin which in our experience induces severe tubular lesions without being lethal (the oxaliplatin and carboplatin doses were adapted to expose all mice to the same amount of Pt) and we chose a

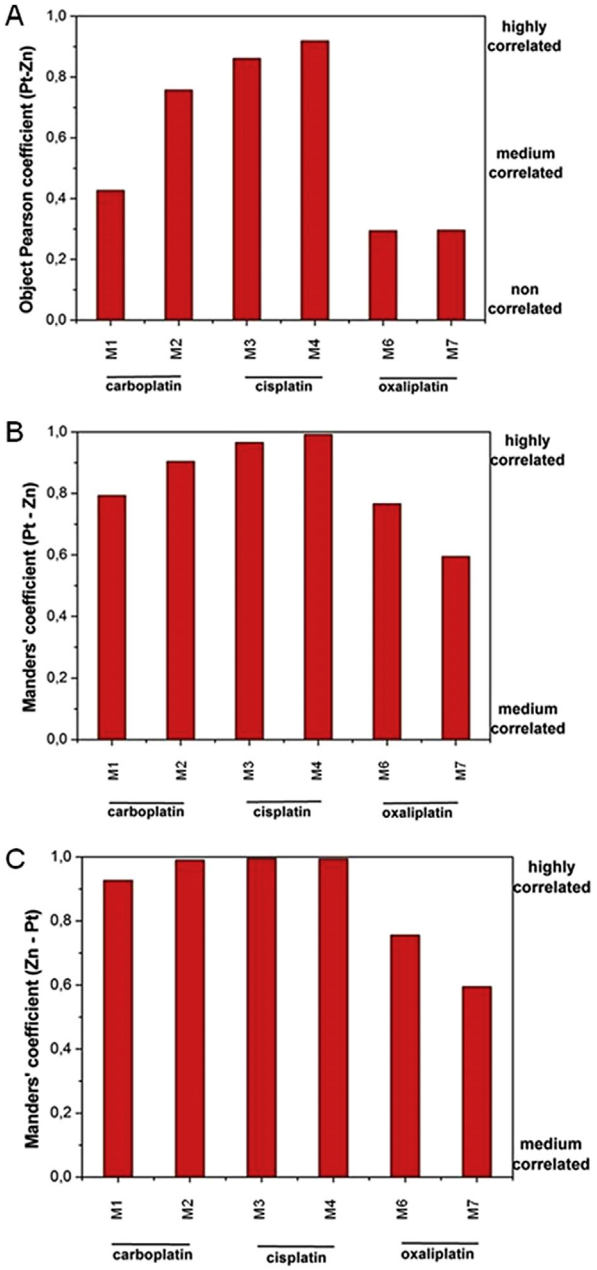

Fig. 3. Correlation coefficients between Zn and Pt obtained through statistical analysis: Pearson (A) and Manders' coefficients (B) and (C). M: Mouse.

time point when renal inflammation is the highest. These experimental conditions were suitable to investigate cisplatin-induced kidney injury but they differ from the clinical situation where the kidney biopsy is usually delayed. The next step will be injection of subtoxic doses of cisplatin to confirm that Zn redistribution to the cortex does correlate with kidney injury. Based on the existing literature on trace elements in normal mouse kidneys [47], we did not analyze a saline injected mouse control. Although SR-μXRF is very sensitive to Pt and Zn in biological tissue, which allows qualitative analyses of their spatial distribution at the micrometer scale, it cannot yet be used as a quantitative tool.

4. Conclusion and perspectives

Our study shows that SR-μXRF is a valuable tool to assess the presence of Pt and Zn in mouse kidneys. These preliminary data seem to reveal that cisplatin induces a specific Zn redistribution pattern which is probably related to its nephrotoxicity. This paves the way for other synchrotron X-rays specific techniques such as EXAFS or XANES to better describe Pt state and surrounding in biological samples. Routine renal pathology laboratories are not equipped to assess the participation of a specific drug in acute kidney injury and investigate the mechanisms of toxicity; μXRF opens new perspectives which hopefully will be translated into improvement of patients' care.

Appendix A. Supplementary data

Supplementary data related to this article can be found at doi:10.1016/j.crci.2016.03.014.

References

[1] J. Ferlay, E. Steliarova-Foucher, J. Lortet-Tieulent, S. Rosso, J.W. Coebergh, H. Comber, D. Forman, F. Bray, Eur. J. Cancer 49 (2013) 1374.
[2] B. Rosenberg, L. Van Camp, J.E. Trosko, V.H. Mansour, Nature 222 (1969) 385.
[3] A.S. Abu-Surrah, M. Kettunen, Current Med. Chem. 13 (2006) 1337.
[4] R.B. Weiss, M.C. Christian, Drugs 46 (1993) 360.
[5] D. Lebwohl, R. Canetta, Eur. J. Cancer 34 (1998) 1522.
[6] E. Wong, C.M. Giandomenico, Chem. Rev. 99 (1999) 2451.
[7] B. Desoize, C. Madoulet, Crit. Rev. Oncol. Hematol. 42 (2002) 317.
[8] H. Zorbas, B.K. Keppler, Chem. Bio. Chem. 6 (2005) 1157.
[9] L. Kelland, Nat. Rev. Cancer 7 (2007) 573.
[10] D. Wang, S.J. Lippard, Nat. Rev. Drug Discov. 4 (2005) 307.
[11] A.V. Klein, T.W. Hambley, Chem. Rev. 109 (2009) 4911.
[12] C. Marzano, F. Bettio, F. Baccichetti, A. Trevisan, L. Giovagnini, D. Fregona, Chemico-Biolog. Interact. 148 (2004) 37.
[13] J. Reedijk, J. Pure Appl. Chem. 59 (1987) 181.
[14] N. Farrell, Transition Metal Complexes as Drugs and Chemotherapeutic Agents, Kluwer Academic Publisher, Boston, 1989.
[15] S.B. Howell (Ed.), Platinum and Other Metal Coordination Compounds in Cancer Chemotherapy, Plenum Press, New York, 1991.
[16] R.K. Jain, Cancer Res. 47 (1987) 3039.
[17] B. Michalke, J. Trace Elem. Med. Biol. 24 (2010) 69.
[18] R.P. Miller, R.K. Tadagavadi, G. Ramesh, W.B. Reeves, Toxins 2 (2010) 2490.
[19] J.T. Hartmann, L.M. Fels, S. Knop, H. Stolt, L. Kanz, C. Bokemeyer, Invest. New Drugs 18 (2000) 281.
[20] J.T. Hartmann, H.-P. Lipp, Expert Opin. Pharmacother. 4 (2003) 889.
[21] J. Sastry, S.J. Kellie, Pediatr. Hematol. Oncol. 22 (2005) 441.
[22] I. Arany, R.L. Safirstein, Semin. Nephrol. 23 (2003) 460.
[23] T. Boulikas, Anticancer Res. 12 (1992) 885.
[24] P. Bonaventura, G. Benedetti, F. Albarède, P. Miossec, Autoimmun. Rev. 14 (2015) 277.
[25] J. Chwiej, K. Fik-Mazgaj, M. Szczerbowska-Boruchowska, M. Lankosz, J. Ostachowicz, D. Adamek, A. Simionovici, S. Bohic, Anal. Chem. 77 (2005) 2895.
[26] C.J. Fahrni, Curr. Opin. Chem. Biol. 11 (2007) 121.
[27] S. Majumdara, J.R. Peralta-Videa, H. Castillo-Michel, J. Hong, C.M. Ricoa, J.L. Gardea-Torresdeya, Anal. Chim. Acta 755 (2012) 1.
[28] S. Bohic, M. Cotte, M. Salomé, B. Fayard, M. Kuehbacher, P. Cloetens, G. Martinez-Criado, R. Tucoulou, J. Susini, J. Struct. Biol. 177 (2012) 248.
[29] D. Bazin, M. Daudon, C. Combes, C. Rey, Chem. Rev. 112 (2012) 5092.
[30] D. Bazin, M. Daudon, P. Chevallier, S. Rouziere, E. Elkaim, D. Thiaudière, B. Fayard, E. Foy, Ann. Biol. Clin. 64 (2006) 125.
[31] E.D. Greaves, M. Angeli-Greaves, U. Jaehde, A. Drescher, A. Von Bohlen, Spectrochim Acta Part B: At. Spectrosc. 61 (2006) 1194.
[32] A.A. Hummer, A. Rompel, Metallomics 5 (2013) 597.

[33] J.Z. Zhang, N.S. Bryce, A. Lanzirotti, C.K.J. Chen, D. Paterson, M.D. de Jonge, D.L. Howard, T.W. Hambley, Metallomics 4 (2014) 1209.
[34] K.J. Davis, J.A. Carrall, B. Lai, J.R. Aldrich-Wright, S.F. Ralph, C.T. Dillon, Dalton Trans. 41 (2012) 9417.
[35] D. Bazin, X. Carpentier, O. Traxer, D. Thiaudière, A. Somogyi, S. Reguer, G. Waychunas, P. Jungers, M. Daudon, J. Synchrotron Radiat. 15 (2008) 506.
[36] D. Bazin, X. Carpentier, I. Brocheriou, P. Dorfmuller, S. Aubert, C. Chappard, Biochimie 91 (2009) 1294.
[37] C. Nguyen, H.K. Ea, Thiaudière, S. Reguer, D. Hannouche, M. Daudon, F. Lioté, D. Bazin, J. Synchrotron Radiat. 18 (2010) 475.
[38] X. Carpentier, D. Bazin, P. Jungers, S. Reguer, D. Thiaudière, M. Daudon, J. Synchrotron Radiat. 17 (2010) 374.
[39] D. Bazin, M. Daudon, C. Chappard, J.-J. Rehr, D. Thiaudière, S. Reguer, J. Synchrotron Radiat. 18 (2011) 912.
[40] D. Bazin, A. Dessombz, C. Nguyen, H.-K. Ea, F. Lioté, J. Rehr, C. Chappard, S. Rouzière, D. Thiaudière, S. Reguer, M. Daudon, J. Synchrotron Radiat. 21 (2014) 136.
[41] P. Kirkpatrick, V. Baez, J. Opt. Soc. Am. 38 (1948) 766.
[42] O. Hignette, P. Cloetens, G. Rostaing, P. Bernard, C. Morawe, Rev. Sci. Instrum. 76 (2005) 063709.
[43] O. Hignette, P. Cloetens, C. Morawe, C. Borel, W. Ludwig, P. Bernard, A. Rommeveaux, S. Bohic, AIP Conf. Proc. 879 (2007) 792.
[44] V.A. Solé, E. Papillon, M. Cotte, Ph. Walter, J. Susini, Spectrochim, Acta Part B 62 (2007) 63–68.
[45] C. Messow, K. Gärtner, H. Hackbarth, M. Kangaloo, L. Lünebrink, Contrib. Nephrol. 19 (1980) 51.
[46] E. Moreno-Gordaliza, C. Giesen, A. Lazaro, D. Esteban-Fernandez, B. Humanes, B. Canas, U. Panne, A. Tejedor, N. Jakubowski, M.M. Gomez-Gomez, Anal. Chem. 83 (2011) 7933.
[47] B. Bao, A.S. Prasad, F.W. Beck, D. Snell, A. Suneja, F.H. Sarkar, N. Doshi, J.T. Fitzgerald, P. Swerdlow, Transl. Res. 152 (2008) 67.
[48] B. Besecker, S. Bao, B. Bohacova, A. Papp, W. Sadee, D.L. Knoell, Am. J. Physiol Lung Cell Mol. Physiol. 294 (2008) L1127.
[49] P.D. Zalewski, A.Q. Truong-Tran, D. Grosser, L. Jayaram, C. Murgia, R.E. Ruffin, Pharmacol. Ther. 105 (2005) 127.
[50] M. Tuzcu, N. Sahin, A. Dogukan, A. Aslan, H. Gencoglu, N. Ilhan, O. Kucuk, K. Sahin, J. Ren. Nutr. 20 (2010) 398.